A Model For Mobile Radio Fading Due to Building Reflections: Theoretical and Experimental Fading Waveform Power Spectra

By JOSEPH F. OSSANNA, Jr.

(Manuscript received May 20, 1964)

Fluctuations in received signal amplitude occur during mobile communications because of the motion of the mobile station through the spatial standing-wave pattern resulting from the interaction of direct and reflected signals. A model is presented which permits a theoretical calculation of the power spectrum of these fluctuations and satisfactorily predicts the features of spectra computed from experimental fading data except for an observed rise at low frequencies.

The model is based on the geometry of the reflections from nearby randomly placed vertical plane reflectors. Vertical polarization is assumed. Both the standing-wave pattern and the Doppler shift view of fading are used to obtain nearly identical results. The detailed shape and in particular the sharp cutoff frequency of the spectrum are shown to depend crucially on the angle α between the direction of vehicle motion and the direction to the fixed station. Detailed comparisons are made of theoretical spectra with experimental spectra representing a range of the angle α.

The collection, digitization, calibration, plotting, and digital processing to obtain power spectra of actual recorded fading waveforms are described.

I. INTRODUCTION AND SUMMARY

The mobile radio fading phenomenon discussed herein is the fluctuation in the received signal amplitude during mobile communication due to the motion of the mobile station through the spatial standing-wave pattern resulting from the interaction of direct and reflected signals. Knowledge of the statistical behavior of such fading signals can permit more meaningful mobile communication system studies and design effort. For example, it can aid in the choice and design of automatic

gain control systems and systems involving data transmission. The particular statistical description of fading to be discussed is the power spectrum of the signal amplitude.

First, this article presents a theoretical model for mobile radio fading due to building reflections, which permits a theoretical calculation of the power spectrum of the fading waveform. Second, the collection, digital processing, and power spectral analysis of actual fading waveforms are described. Then detailed comparisons are made between the theoretical and experimental spectra. Limitations and extensions of the model are explored.

Historically, the evolution of the model followed a study of the power spectra of fading waveforms recorded on one particular street. These spectra had an unexpected and interesting shape. The model indicated that the shape of the spectrum and particularly the frequency at which the power density fell abruptly would depend on the vehicle's direction of travel with respect to the direction toward the fixed station. Subsequent fading waveforms, recorded on other streets having various relative directions, produced power spectra which collectively exhibited all the features predicted by the model.

1.1 *Characteristics of Experimental Power Spectra*

Fading waveforms were recorded on 13 streets in New Providence, N. J. on Sept. 13, 1962, using a carrier frequency of 838 mc and a nominal vehicle speed of 15 mph. Vertical polarization was used. The fade rate corresponding to motion through standing-wave minima a half-wavelength apart is 37.5 cps. After digitization, calibration, and smoothing, power spectra were computed. Almost all of these spectra exhibited: (1) a very sharp cutoff at a frequency somewhere between 20 and 40 cps, followed, after a drop of between 10 and 20 db, by a 12 db/octave fall-off; (2) a narrow peak between 3 and 10 db high just prior to the sharp fall; (3) a broader, shorter intermediate peak; and (4) a rise at the low-frequency end of 10–15 db. Many spectra exhibited a shelf in the frequency range between the sharp fall and the gradual fall-off which extended to about twice the sharp-fall frequency. Other sometimes subtle features were noted which will be mentioned later.

1.2 *The Model*

The simple model to be described predicts a theoretical power spectrum for the fading waveform having all the features of a corresponding experimental spectrum except a low-frequency rise. In particular, the

frequency, shape, and size of two peaks, the sharp fall, the following shelf, and the subsequent gradual fall-off are satisfactorily predicted.

The model is based on the geometry of the reflections from nearby randomly placed, vertical, plane, good reflectors. Vertical polarization is assumed (the use of horizontal polarization is discussed in Section XIV). The vehicle is assumed to move through the standing-wave pattern caused by the reflections. A virtually identical result obtains if the vehicle is assumed to encounter appropriate Doppler shifts for each reflected signal. The computed spectrum depends on: (1) the radio carrier frequency, (2) the vehicle speed, and (3) the angle α between the vehicle direction of motion and the direction to the fixed station.

If f_m is the fade frequency which would be experienced by the vehicle moving directly across standing-wave minima spaced $\lambda_c/2$ apart (λ_c = carrier wavelength), the model indicates that the spectrum will peak and then fall sharply at some frequency f_p between $f_m/2$ and f_m and that an intermediate peak will occur at a frequency $f_m - f_p$. In terms of the angle α defined in the previous paragraph, f_p is equal to the larger of $f_m \sin^2 \alpha/2$ or $f_m \cos^2 \alpha/2$. As α varies between 0 (or 180°) and 90°, f_p varies between f_m and $f_m/2$.

1.3 *Comparison between Experimental and Theoretical Spectra*

Because the angle α varies during a typical data run along any street, theoretical spectra were determined by averaging spectra computed for sample α's along the run. The agreement between experimental and theoretical spectra is generally quite good. The sharp-fall frequency agrees perfectly in almost all cases. Other details are in good agreement in many cases. The main discrepancy is the absence of a theoretical forecast of the rise in the observed spectral density at low frequencies. One street which, unlike all the others, had few buildings produced experimental spectra only vaguely similar to theoretical expectations. Mechanisms not considered in the theoretical model which would contribute low-frequency energy include: (1) shadowing by buildings, (2) variations in and the shadowing of ground reflections, (3) the intermodulation of concurrent reflections and (4) nonrandom reflector orientation.

1.4 *Usefulness of Model*

The model in the form offered successfully predicts fading waveform power spectra in a suburban residential environment. The possibility certainly exists that an extension of the model can be made to work

elsewhere. The usefulness of power spectra is not unlimited, and many statistical properties of fading cannot easily be deduced from spectra. One of the main values of the agreement between these theoretical and experimental spectra is its verification of the physical basis of the model.

II. THE MODEL

We will begin by considering the fading experienced by a mobile receiver moving through a standing-wave pattern due to a single reflector when the transmission is vertically polarized. Reciprocity will insure application of the results to the case where the receiver is fixed and the transmitter is moving. First, the fade rate will be related to the vehicle trajectory. Then the same result will be obtained using the Doppler point of view. Then the relative contribution from reflectors in different directions will be determined. Next, a theoretical spectrum will be constructed for the case of many reflectors; its shape will depend strongly on the vehicle direction relative to the fixed station.

III. STANDING-WAVE PATTERN DUE TO A SINGLE REFLECTOR

If the mobile antenna is a fixed height above the ground, only the larger (many wavelengths) vertical plane reflectors in the vicinity of the mobile station are of major importance in determining the local standing-wave pattern fluctuations. Reflectors of ordinary size which are not in the vicinity of either the mobile or fixed stations are of lesser importance because their reflected signals will be of smaller amplitude. Reflectors near the fixed station can contribute large amplitude reflections, but their effect is more that of modifying the directivity pattern of the fixed antenna; their effect is to put slow multiplicative trends into the standing-wave pattern at the mobile station. Furthermore, fixed station antennas are usually mounted above local obstacles that would not only reflect but shield some direction.

We will assume that the transmitting and receiving antennas are vertically polarized. Then the local standing-wave pattern due to a single vertical plane conducting reflector is as shown in Fig. 1 where:

φ = angle between the direction to the fixed station and the direction to the reflector as seen from the mobile antenna,

α = angle between the direction to the fixed station and the direction of vehicle travel,

θ = angle of incidence at the reflector,

d = perpendicular distance between null planes,

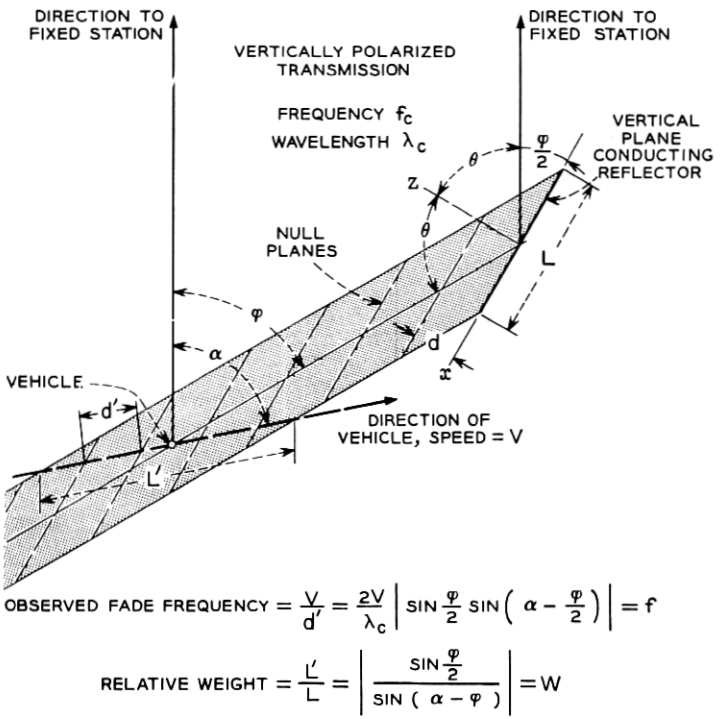

Fig. 1 — Vehicle moving through standing-wave pattern due to single reflector.

d' = spacing between null planes observed along direction of mobile station travel,
L = length of reflector,
L' = length of vehicle path in reflected beam, and
λ_c = carrier frequency wavelength.

The fixed station is assumed to be far enough away to permit taking the incident waves on the mobile antenna and on the reflector as parallel. The reflector is assumed to be large compared to a wavelength ($L \gg \lambda_c$) and close enough to the mobile station to neglect divergence of the reflected beam.

3.1 *Null Plane Spacing*

Note that a reflector in a direction φ must be oriented such that

$$\theta + (\varphi/2) = 90^\circ \tag{1}$$

for the reflected beam to be directed toward the mobile station (for the

angle of reflection to equal the angle of incidence). To determine the spacing d between null planes, refer to Fig. 2 and observe that

$$a - b = \lambda_c , \tag{2}$$

$$b/a = \cos \varphi, \tag{3}$$

and

$$d/a = \sin (\varphi/2). \tag{4}$$

From (2) and (3), a is found to be

$$a = \frac{\lambda_c}{1 - \cos \varphi} = \frac{\lambda_c}{2 \sin^2 \frac{\varphi}{2}} . \tag{5}$$

Then (4) and (5) yield

$$d = a \sin \frac{\varphi}{2} = \frac{\lambda_c}{2 \sin \frac{\varphi}{2}} , \tag{6}$$

or, using (1)

$$d = \frac{\lambda_c}{2 \cos \theta} . \tag{7}$$

This is of course a common result (see Ref. 1, p. 293 ff.).

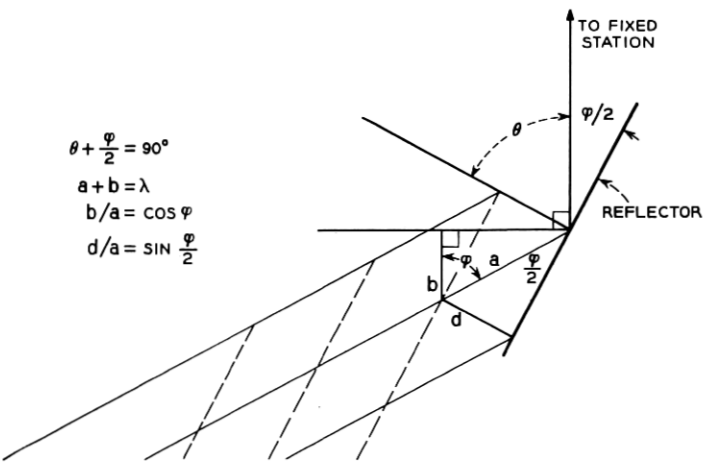

Fig. 2 — Portion of Fig. 1 in vicinity of reflector.

3.2 *Fading Rate*

Because of its direction of travel, the mobile antenna observes a null spacing d', which from Fig. 3 is

$$d' = \frac{d}{\sin\left(\alpha - \frac{\varphi}{2}\right)}, \tag{8}$$

which by using (6) becomes

$$d' = \frac{\lambda_c/2}{\sin\frac{\varphi}{2}\sin\left(\alpha - \frac{\varphi}{2}\right)}, \tag{9}$$

which holds for the case where $\alpha > \varphi/2$. Consideration of various values for α and $\varphi/2$ leads to the general relation

$$d' = \frac{\lambda_c/2}{\left|\sin\frac{\varphi}{2}\sin\left(\alpha - \frac{\varphi}{2}\right)\right|}. \tag{10}$$

If the vehicle speed is V, the fading frequency is

$$f' = \frac{V}{d'} = \frac{2V}{\lambda_c}\left|\sin\frac{\varphi}{2}\sin\left(\alpha - \frac{\varphi}{2}\right)\right|. \tag{11}$$

Then f' has the maximum value $f_m' = 2V/\lambda_c$, where $\varphi = 180°$ and

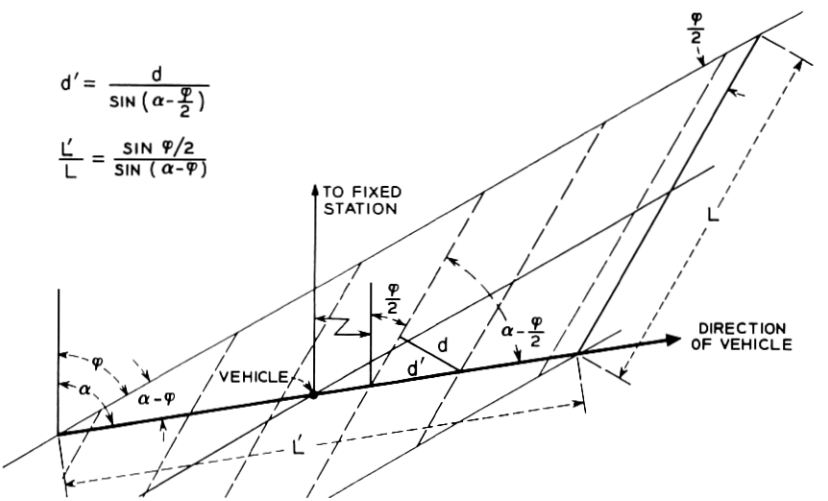

Fig. 3 — Portion of Fig. 1 in vicinity of receiver.

$\alpha = 0°$ or 180°, when the vehicle moves perpendicularly across null planes spaced $\lambda_c/2$ apart. For $f_c = 838$ mc and $V = 15$ mph, $f_m' = 37.5$ cps. For convenience, we will usually use a normalized fading frequency $f = f'/f_m'$. When $\alpha \neq 0°$ or 180°, f is zero at $\varphi = 0$, 2α, and 360°, and has the maximum values $f_1 = \sin^2(\varphi/2)$ at $\varphi = \alpha$ and $f_2 = \cos^2(\varphi/2)$ at $\varphi = 180 + \alpha$; note that $f_1 + f_2 = 1$. Thus, for a particular α, the maximum possible fade rate is $f_{\max} = \max(f_1, f_2)$* and is due to a vehicle motion either toward or away from a reflector. The minimum possible value for $f_{\max}$ occurs when $f_1 = f_2 = \frac{1}{2}$, which corresponds to $\alpha = 90°$. The variation of f with φ is shown in Fig. 4 for $\alpha = 0°$, 30°, 60°, and 90°.

3.3 *Fading Waveform*

If the reflector is perfectly conducting as assumed above, the actual waveform observed at the output of an envelope detector in the mobile vehicle would be the familiar result of beating two frequencies of equal amplitude — a full-wave rectified sine wave. Thus, in addition to the fundamental fade rate discussed above, significant harmonics will also be present. If the reflector is not perfectly conducting or is only a dielectric, minima will occur instead of nulls; the spacing between them will remain the same as for the nulls, and the waveform will tend to be more nearly sinusoidal.

IV. THE DOPPLER POINT OF VIEW

We can instead consider fading as due to the beating within the receiver of different carrier frequencies arising from the different Doppler shifts occurring for the directly incident and reflected waves. The carrier frequency observed at the vehicle will in general be

$$f_o = f_c + (v/\lambda_c) \tag{12}$$

where f_c and λ_c are the transmitted carrier frequency and wavelength and v is the relative velocity of closure between the two stations. From Fig. 1, the observed frequency of the directly incident signal is

$$f_i = f_c + \frac{V \cos \alpha}{\lambda_c}, \tag{13}$$

where V is the vehicle speed.

* Max (a,b,c, $\cdots$) = the algebraically largest of the sequence a,b,c, $\cdots$. Similarly, min (a,b,c, $\cdots$) = the algebraically smallest of a,b,c, $\cdots$.

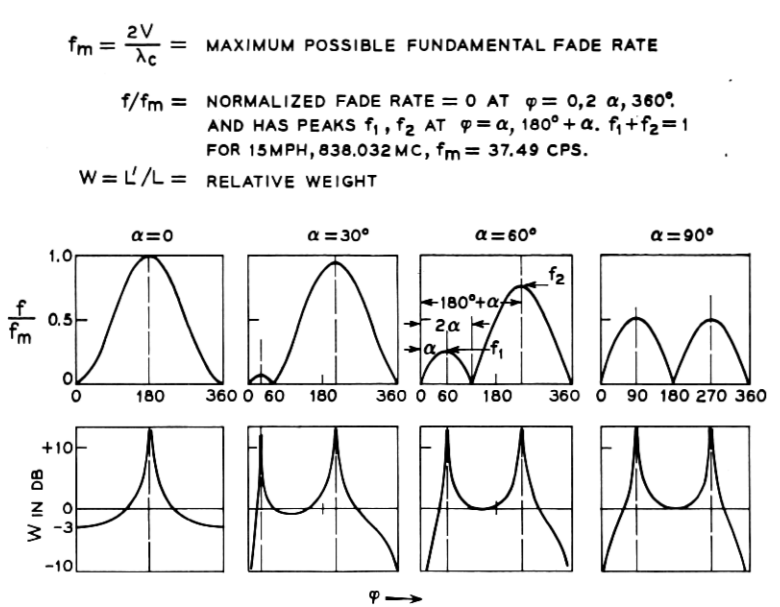

Fig. 4 — Variation of fade frequency f and weighting function W with relative vehicle direction α and relative reflector direction φ.

The observed frequency of the reflected signal is

$$f_r = f_c + \frac{V \cos(\alpha - \varphi)}{\lambda_c}. \tag{14}$$

The fading rate will then be the beat frequency between f_i and f_r:

$$f = f_r - f_i = \frac{V}{\lambda_c}[\cos(\alpha - \varphi) - \cos\alpha] \tag{15}$$

$$= \frac{V}{\lambda_c}[\sin\alpha \sin\varphi - \cos\alpha(1 - \cos\varphi)]$$

$$= \frac{V}{\lambda_c}\left(2\sin\frac{\varphi}{2}\right)\left[\sin\alpha\cos\frac{\varphi}{2} - \cos\alpha\sin\frac{\varphi}{2}\right]$$

$$= \frac{2V}{\lambda_c}\left[\sin\frac{\varphi}{2}\sin\left(\alpha - \frac{\varphi}{2}\right)\right]. \tag{16}$$

After absolute value signs are added to (16) to account for the various relative values of α and φ, the result is identical to (11).

The Doppler point of view has one important advantage over the standing-wave pattern point of view. It is easier to see what fade rates

will occur when more than one reflector is involved; when n reflectors are simultaneously effective, $n(n + 1)/2$ beat frequencies are possible.

V. THEORETICAL POWER SPECTRUM

Since the observed fading rate is a function of the parameters α and φ discussed above, the power spectrum of the fading waveform at the output of an envelope detector in the mobile vehicle will evidently be a function of time, even if the vehicle speed is constant. In this section, we will develop an approximation to the power spectrum of a finite duration of fading waveform. We will assume: (1) the vehicle speed is constant; (2) the transmission is vertically polarized; (3) an unmodulated carrier is being transmitted; (4) the reflectors are large, stationary, vertical, plane conductors; and (5) only reflectors in the vicinity of the mobile vehicle are important. Other assumptions inherent in the development will be stated when appropriate.

5.1 *More Than One Reflector*

A major step in simplifying the analysis is to assume that, although many reflected beams will be encountered by the vehicle during the finite run, only one such beam is important at any one time. This eliminates the necessity of considering beats between reflections. The effect of this assumption on the theoretical spectrum will be discussed later. Actually, there is a strong tendency for this assumption to be true in a suburban residential environment because the houses are well spread out.

5.2 *The Relative Importance of Different Reflectors*

The energy in a particular small frequency band in the finite sample of fading waveform will be proportional to the time that frequencies in that band are present. The corresponding power spectral density will be proportional to the corresponding fraction of the total run time. Thus the contribution of a particular reflector to the appropriate frequency band will be proportional to the time it takes the vehicle to cross the reflected beam or, if the vehicle speed is constant, proportional to the length of its path through the beam, which is the length L' in Fig. 1.

If we assume that all the reflectors are the same size (L in Fig. 1), then the contribution of a particular reflector to the power spectrum will be proportional to a weighting function $W = L'/L$. The assumption of equal-size reflectors is another assumption that has a strong tendency to be true in suburban residential areas, where all the houses

in a given locale tend to be the same size. From Fig. 3 it is evident that

$$W = \frac{L'}{L} = \frac{\sin(\varphi/2)}{\sin(\alpha - \varphi)}. \tag{17}$$

Consideration of the various values of α and φ yields the general result

$$W = \frac{L'}{L} = \left| \frac{\sin \varphi/2}{\sin(\alpha - \varphi)} \right|. \tag{18}$$

Because L' cannot exceed the total run length L_T, the physical maximum value of W is $W_{\max} = L_T/L$. Fig. 4 shows the variation of W with φ for $\alpha = 0°, 30°, 60°$, and $90°$; the plots of W, which are in db ($10 \log_{10} W$) are shown directly below corresponding plots of the fade rate f. W has the value zero ($-\infty$ db) at $\varphi = 0°$ (and 360°), except when $\alpha = 0$ where $W = 0.5$ (-3 db) at $\varphi = 0°$. $W = 1$ (0 db) at $\varphi = 2\alpha$. And W is truncated to $W_{\max}$ at $\varphi = \alpha$ and $180° + \alpha$; the peaks of W are coincident with the peaks of the fade rate f. Not only do the reflectors directly ahead or behind the vehicle cause the most rapid fades, but they are the most important contributors to the power spectrum.

It is interesting to note that the weighting function W can be arrived at in another way. Consider the portion of the f vs φ curve between $\varphi = 0°$ and $\varphi = \alpha$. The small range of reflector directions $d\varphi$ contributing to a small frequency band df can be found by differentiating (11) to get

$$df/d\varphi = \tfrac{1}{2} \sin(\alpha - \varphi). \tag{19}$$

The projected length of a reflector in a direction φ is $L_p = L \cos \theta = L \sin \varphi/2$ (assuming L constant). Suppose that the contribution to the power in a band df due to the reflectors in a range $d\varphi$ is

$$P(f)df = C \frac{d\varphi}{2\pi} \cdot \frac{L_p}{L}, \tag{20}$$

where C is a constant. Substituting for $d\varphi/df$ and L_p/L then gives

$$P(f) = \frac{C}{\pi} \frac{\sin \varphi/2}{\sin(\alpha - \varphi)}, \tag{21}$$

which except for the constant is identical to (17).

5.3 *The Theoretical Spectrum Method*

Consider again the plots of fade rate f vs φ shown in Fig. 4. For any particular $f < f_{\max} = \max(f_1, f_2)$, there are either two or four corresponding values of reflector directions φ. For each of these φ's the

corresponding value of the weighting function can be found from (18) and is seen on the W vs φ plot directly under the f vs φ plot. We will assume that the mobile station is under the influence of one reflector at a time; this condition has a strong tendency to be true in suburban residential areas. Then, if we further assume that all reflector directions are equally likely, the power density at the frequency f will be proportional to the sum of the two or four values of W.

The basic procedure for generating a theoretical spectrum for comparison with a spectrum computed from experimental data is, if α is constant:

(*i*) Select a list of frequencies $f = n\Delta f$, where $\Delta f = (f_{\text{fold}}/M)/(2V/\lambda_c)$ and $n = 0,1,2 \cdots$; f_{fold} is the folding frequency (Ref. 2, p. 117 ff.) of the experimental data, M is the number of lags (Ref. 2, p. 120 ff.) used in computing its spectrum, and $(2V/\lambda_c)$ is the corresponding f_m'. In other words, select the same frequencies, normalized by dividing by f_m', at which spectral estimates were computed for the experimental data. The reason for this matching of frequencies will be discussed below.

(*ii*) For each frequency, determine the two or four reflection directions φ, using (11) or Fig. 4. Then for each frequency determine the corresponding two or four weighting functions W from (18); each W should of course be limited to $W_{\max}$.

(*iii*) At each frequency, sum the two or four corresponding values of the weighting function W to get the spectral power density.

The solution of (11) in step (*ii*) above can be accomplished by Newton's iteration procedure. Also, the symmetry of the f vs φ function about $\varphi = \alpha$ and $180 + \alpha$ can be used; if $\varphi_1 < \alpha$ is a solution, $\varphi_2 = 180 - \varphi_1$; and, if $2\alpha < \varphi_3 < 180 + \alpha$ is another solution, $\varphi_4 = 360 + 2\alpha - \varphi_3$. In the case where $\alpha = 0$ (or 180°) an explicit solution for the two φ's and the sum of the two W's can be obtained. Setting $\alpha = 0$ in (11) gives

$$\frac{f'}{f_m'} = f = \sin^2 \frac{\varphi}{2}, \tag{22}$$

and the solution $\varphi/2 = \arcsin f^{\frac{1}{2}}$. Setting $\alpha = 0$ in (18) gives

$$W = \left| \frac{1}{2 \cos \varphi/2} \right|. \tag{23}$$

Because (23) is symmetrical about $\varphi = \pi/2$, the two W's are equal, and (22) and (23) combine to give the spectral density as

$$P(f) = \min\left(2W_{\max}, \frac{1}{\sqrt{1-f}}\right), \tag{24}$$

where the physical limit on W is included.

Implicit in the procedure thus far is the assumption that fading waveform contributed by each reflector is sinusoidal. The resulting power spectrum is zero above $f_{\max}$. Actually, the fading waveform due to a single reflector has an harmonic content which depends on the relative amplitudes of the direct and reflected signals; when one is much smaller than the other the fading tends to be sinusoidal, and when they are equal the fading waveform is a full-wave rectified sine wave. This can be seen by superposing the incident and reflected electric field components; in terms of the z coordinate of Fig. 1, the resultant electric field of a vertically polarized wave has the form (see Ref. 1, p. 296)

$$|E| = \left|K \sin\left(\frac{2\pi z}{\lambda_c} \cos\theta\right)\right|, \tag{25}$$

where K is a constant and θ is the angle of incidence. The spectra of the experimental data all exhibit fall-offs subsequent to the fall corresponding to $f_{\max}$. The harmonic content of the fading can be included in the theoretical spectrum by determining the harmonic power corresponding to each original theoretical spectral estimate and adding this power in at the corresponding set of harmonic frequencies. Arbitrarily, the coefficients for a full-wave rectified sine wave were used to determine the relative power at the harmonic frequencies; this will provide a maximum of harmonic power. It is an interesting fact that inclusion of harmonic power does not significantly alter the shape of the theoretical spectrum at frequencies below $f_{\max}$.

The final step in generating the theoretical spectrum is to smooth it in an appropriate way. Because the spectra computed from experimental data are estimates of smoothed versions of the true power spectra (see Ref. 2), the theoretical spectra should be smoothed in a corresponding way. Therefore the theoretical spectra to be shown will have been smoothed by hanning.[2] This is the reason for matching the theoretical and experimental spectral estimate frequencies.

Finally, if the relative path angle α varies during the run, its variation can be represented by a weighted list of sample α's. The spectrum for each α can be determined and the resulting spectra averaged. The smoothing can be done after averaging.

5.4 *Theoretical Spectra for Various Constant α's*

Fig. 5 shows theoretical spectra for $\alpha = 0°$, 30°, 60°, and 90°, $V = 15$ mph, $f_c = 838$ mc, and $W_{\max} = 15$. The corresponding $f_m' = 37.5$ cps. Consider first the curve for $\alpha = 60°$. The peaks corresponding to the relatively heavily weighted frequencies in the vicinity of f_1 and f_2 ($f_1' = 9.4$ cps, $f_2' = 28.1$ cps) are clearly evident. Following f_2', the power density falls sharply and levels off abruptly to form a shelf. The shelf, which arises primarily from second-harmonic power, peaks around 56 cps prior to a second sharp fall. Following the second-harmonic shelf is one due primarily to third harmonics which ends at about 84 cps. Because the points in the fundamental frequency portion of the spectrum

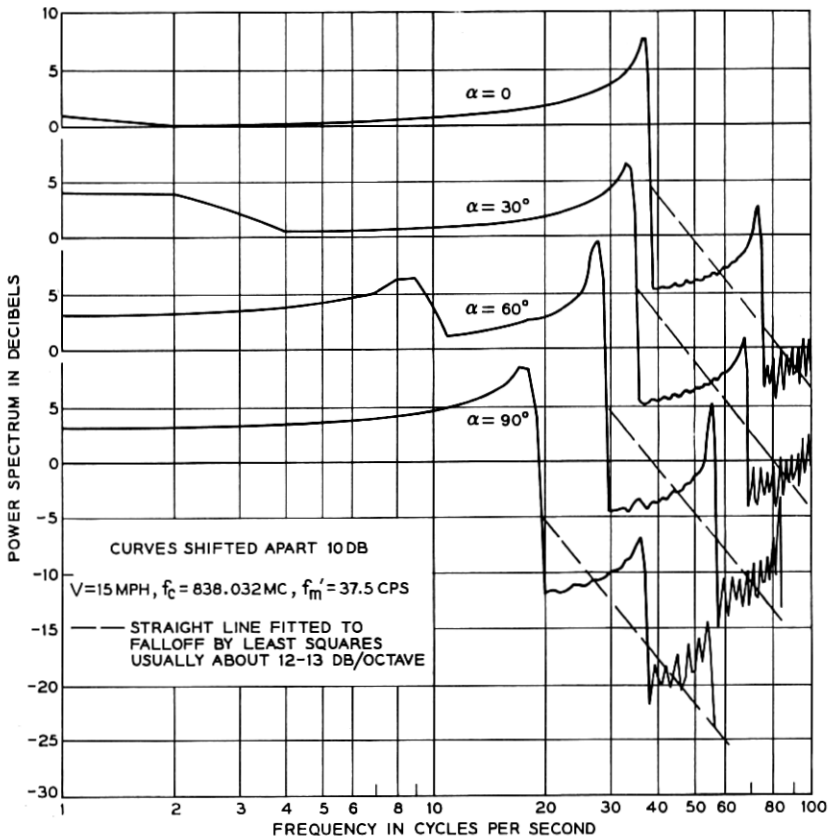

Fig. 5 — Theoretical fading waveform power spectrum vs relative vehicle direction α. Theoretical spectral estimates are 1-cps apart.

were computed at 1-cps spacings, the harmonic shelves get increasingly jagged-looking at higher frequencies. The dashed line sloping down through the shelves is a least squares straight-line fit to the portion of the spectrum following the first sharp fall. The falloff line in the $\alpha = 60°$ case has a slope of -13.0 db/oct.

The peaks in the $\alpha = 30°$ case correspond to $f_1' = 2.5$ cps and $f_2' = 35.0$ cps. When $\alpha = 0$, $f_1' = 0$ and $f_2' = 37.5$ cps. And when $\alpha = 90°$ the peaks unite at $f_1' = f_2' = 18.75$ cps. The least square fall-off lines have slopes that generally fall between 12–13 db/oct.

5.5 *Theoretical Spectra for α Uniformly Distributed*

Fig. 6 shows the result of averaging the spectra for α's uniformly distributed 0–360° (spectra for $\alpha = n2°$, $n = 0, 1, \cdots, 45$, were averaged). The spectral density is quite flat out to 37.5 cps, where it drops abruptly about 16 db to the second-harmonic shelf. The harmonic shelves in this case are also quite flat. The least squares fall-off line is shown and has a slope of -13.2 db/oct.

VI. DATA COLLECTION

The fading waveforms due to vehicle motion were recorded (on FM tape with an Ampex FR100) for 17 runs on 13 different streets (runs on some streets were made in both directions) in New Providence, N. J., on Sept. 13, 1962. Transmission at 838.032 mc was from the mobile

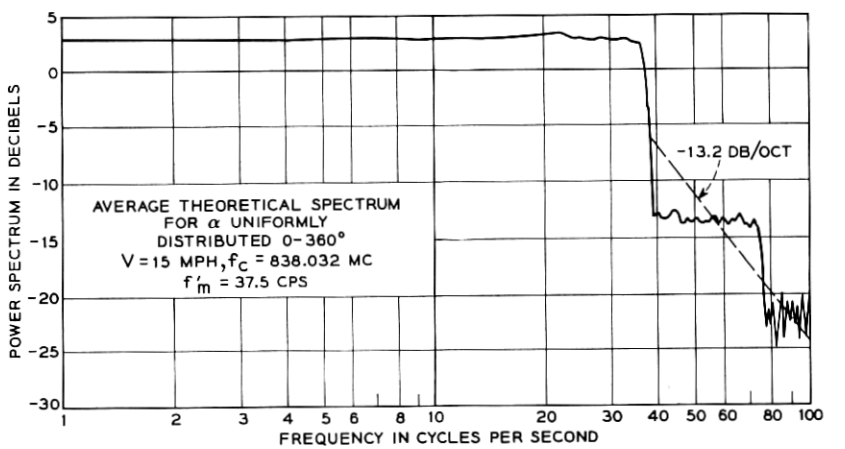

Fig. 6 — Average theoretical power spectrum for a uniform distribution of relative vehicle direction α.

vehicle (a Volkswagen Kombi) traveling nominally 15 mph, to a fixed station at the Murray Hill Laboratories. The range was between 1 and 2 miles and varied little during any run. The duration of the recorded waveforms ranged from about 20 to 150 seconds. Values obtained for the parameter angle α ranged from 6° to 90°. All of the streets were in suburban residential areas except Central Avenue, which serves open fields and a few single-story industrial and commercial buildings. The weather was clear and dry.

The vertically polarized transmitting antenna atop the vehicle was a stack of $2\frac{1}{2}$ coaxial dipoles with a net gain of about 4.5 db. The interaction with a second similar antenna several wavelengths away is not known, but is believed to be small. The receiving antenna was a vertically polarized 13-element coaxial array mounted atop a rooftop elevator house. It had about 11 db gain and a 3-db beamwidth of about 6°.

A voice channel was recorded simultaneously with the fading signal on a second FM tape channel. This channel carried a running commentary describing the data and included start- and end-of-data announcements. Also recorded on this same channel were tone bursts triggered every nominal 0.01 mi by a cam attached to the speedometer cable. The exact vehicle speed was ultimately recovered from these bursts.

To permit over-all calibration of the static transfer characteristic of the system, calibration levels 3 db apart over a 60-db range were recorded both prior and subsequent to the recording of the fading signals. The two stations were directly connected by coax for calibration. Each level was recorded for a few seconds along with appropriate voice announcements.

A complete set of Visicorder records were then made from the FM magnetic tape of both the fading signals and the tone bursts for a preliminary examination of the data and for later determination of the vehicle speeds.

The pertinent parameters for data runs whose power spectra are shown in this article are given in Table I. The system bandwidth was limited by the receiver, which was 3 db down at 310 cps. The angular elevation above the horizon of the fixed station as viewed from the mobile station was usually between 1° and 3°.

6.1 *Vehicle Speed*

Four timed test runs were made in the vehicle over a fixed, level course of 1443 ft., to determine typical speed variations during a run and

TABLE I — PARAMETERS OF RECORDED DATA FOR WHICH COMPARISONS ARE SHOWN BETWEEN THEORETICAL AND EXPERIMENTAL SPECTRA*

Case No.	Street	Avg. Speed mph	Alpha (deg)			f'_{max} cps	f'_m cps	Fig. No.
			min	max	avg.			
1	Commonwealth	15.8	82.2	84.5	83.3	22.4	39.5	10
2	Charnwood	15.8	73.0	75.8	74.4	25.5	39.5	11
3	Whitman	15.2	67.8	80.4	74.2	26.2	38.0	12
4	Elkwood	16.2	41.0	42.6	41.8	35.4	40.4	13
5	Ridgeview	15.8	167.8	168.4	168.1	39.2	39.6	14
6	Ridge	15.9	15.0	15.8	15.4	38.9	39.7	15
7	Central	16.0	68.7	72.9	70.8	27.2	39.9	16

* All spectra were computed using 5000 sample points (20 sec at 250 points/sec).

to calibrate the tone burst rate. The nominal speed for each run was 15 mph = 22 ft./sec. Visicorder recordings were made of the bursts from the FM tape to enable counting them and measuring their spacing; the Visicorder paper speed was determined to be 1.019 in./sec using a 10-cps square wave (set by frequency counter). The tone burst rate was found to be 51.98 ± 0.16 ft. between beginnings of bursts. Using this burst rate, the averages and standard deviations of the speed during these four runs are shown in Table II.

The actual average vehicle speed during each data run or part of a run was determined from the Visicorder records which have the tone bursts plotted alongside the fading signal. Let N_B be the number of bursts occurring during a part of the run and D_R (inches) be the corresponding length of Visicorder paper. The average vehicle speed S_R for that part of the run was then computed from $S_R = 53.0\ N_B/D_R$ ft./sec.

6.2 *Location of Data Runs*

The precise location of each run was carefully marked on a set of topographic maps (100 ft = 1 inch) which showed actual street and house shapes. Typically, street intersections and poles were used as starting and ending points. Except in the case of Whitman Road, which is slightly S-shaped, the vehicle was driven in a straight line.

VII. PATH TRAJECTORY DATA

The set of topographic maps referred to previously have a common coordinate grid. By determining the coordinates of the starting and

TABLE II — AVERAGES AND STANDARD DEVIATIONS OF SPEEDS DURING FOUR TEST RUNS

Test Run	Avg. Speed (ft./sec)	Std. Dev. (ft./sec)
1	23.15	0.63
2	23.08	1.09
3	23.16	0.54
4	23.43	0.41
Average	23.21	0.67

ending points of each run, and the coordinates of the fixed station, it is possible to compute the vehicle azimuth (path azimuth), the azimuth of the direction from the fixed station to the mobile station (fixed azimuth), the angle α between the direction of the vehicle and the direction to the fixed station (positive if fixed station is to the left of the vehicle), and the range at various points along the run. Except in the case of Whitman Road, the end points were connected with a straight line which was then divided into 50-ft. intervals (the last interval usually extending past the original end point). The value of α was then tabulated for the distances $n50$ ft. ($n = 0,1,2, \cdots$) along each run. It should be noted that even with a straight path α varies because of the finite distance to the fixed station.

In the case of Whitman Road, where the path trajectory follows the shape of the road and is not straight, a larger map (50 ft. = 1 in.) was used which showed the actual azimuth variation along the street.

VIII. DIGITAL PROCESSING

Following digitization of the fading data, the calibration, plotting, filtering and spectral analysis were accomplished on an IBM 7094. Many computer programs and subroutines were written for these purposes as well as for such auxiliary purposes as calibration curve fitting, magnetic tape searching (subroutines that can conveniently retrieve requested data pieces), spectra equalizing and plotting, and vehicle path angle determination. An available set of time series processing subroutines[3] was extensively used; this set included subroutines for tapering and detrending data, and for computing auto- and cross-covariances and Fourier transforms. A large arsenal of subroutines was eventually amassed, and writing a program for some particular task became the relatively simple job of writing a program to call appropriate subprograms.

IX. INITIAL DATA PROCESSING

9.1 *Digitization*

Both the fading waveforms and the recorded fixed calibration levels were digitized on an analog-to-digital converter within the Laboratories,[4] using 11 bits/sample and sampling at 500 cps. The procedure for digitizing consisted of playing back the analog tape, listening to the voice-channel announcements, and manually triggering the digitizer on and off at the indicated times. Approximately 2-second intervals of each calibration level were digitized. The signals were filtered prior to sampling by a passive filter which was 3 db down at 250 cps, 10 db down at 300 cps, and subsequently fell 36 db/octave. The folding or Nyquist frequency (see Ref. 2, p. 30 ff.) of $500/2 = 250$ cps was chosen to safely contain the expected power spectra.

9.2 *Microfilm Plotting*

The digital data was read into the 7094 and completely plotted on microfilm on a peripheral General Dynamics 4020 microfilm printer. This provided a good visual record of the raw data as well as a check on the digitizing process. A computer subroutine was developed which generates a long continuous plot down the length of the microfilm. Such plots were produced for monitoring after every step in processing or transcribing the data. The comparative ease with which large quantities of digital data can be monitored by viewing microfilm considerably reduces the chance of the accidental processing and use of data containing errors. The 17 runs of recorded fading waveforms, which totaled over 920 seconds, yielded over 460,000 data points when digitized at 500 cps. When plotted at 480 points per 35 mm frame, the complete data comprising 960 frames could be viewed in detail on a roll film viewer in about an hour. Fig. 7, which exhibits a typical data section, was traced from a print from one frame of microfilm.

9.3 *Calibration*

The communication system nonlinearities, including that of the linear-to-log converter used during analog recording, had to be removed to obtain true signal amplitude. The before and after (the data) sequences of calibration level records were read on the 7094, and each record was averaged to remove noise and obtain a calibration point. Any system net drift during original data recording or during digitization would

make the before and after curves different. Fortunately, they were quite similar and they were averaged to obtain the adopted calibration curve. A suitable function was then fitted, using a least squares criterion, to the list of calibration points. The adopted calibration function is

$$Y = -60.255 + 0.8282\,(X - 170.6)^{\frac{1}{2}} - 0.01614\,(X - 170.6) + 8.474\cdot 10^{-6}\,(X - 170.6)^2 - 9.658\cdot 10^{-10}\,(X - 170.6)^3, \tag{26}$$

where X is the digital sample value and Y is the true signal in relative db. This function, which has a maximum error of 0.47 db near $Y = -3$ db and rms error of 0.21 db, is shown in Fig. 8 plotted along with the original calibration points. Input values outside expected limits of $X = 170.60$ and 4041.06 were clipped to these values. The calibration program kept a statistical history of any clipped regions. The signal amplitude is then exp $(0.11512926Y)$.

X. INITIAL ANALYSIS AND SECOND-STAGE PROCESSING

10.1 *Preliminary Power Spectra*

These were computed for several pieces of the data to determine whether any smoothing and decimating [Ref. 2, pp. 129–135] was

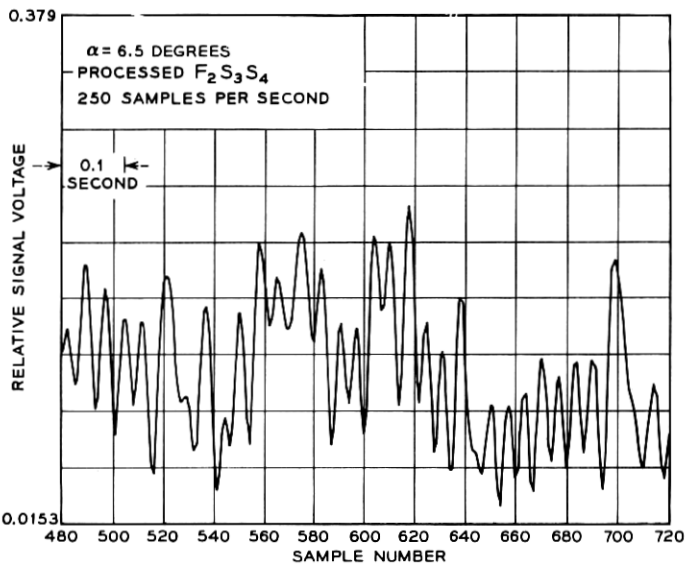

Fig. 7 — Typical section of data.

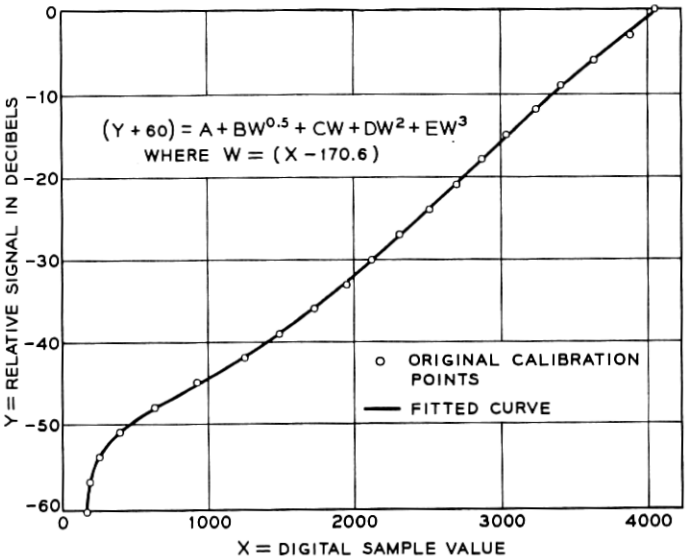

Fig. 8 — Original calibration points and fitted curve from (26).

necessary or desirable. The power spectra computation will be discussed later. Being sure to pick runs expected to have the widest band spectra, it was determined that the significant portions of the spectra were safely below one-half the folding frequency of 250 cps. Decimation by two (retaining every other point), which would reduce the folding frequency to 125 cps, would be safe and would reduce computation time. Suitable smoothing prior to decimating can also remove or reduce the 120-cps and higher hum peaks which were observed. Removing this hum is not essential for the spectral analysis, but doing so makes the data more suitable for level crossing analysis.

10.2 *Smoothing and Decimating*

The decimation of data retaining every Jth point, symbolically indicated by F_J, multiplies the folding frequency by $1/J$. To prevent power, including noise power and hum power, at frequencies above the new lower folding frequency from folding over and appearing below this frequency, the data must be smoothed (or filtered) before decimation (see Ref. 2, pp. 129–135).

The most economical type of smoothing in digital analysis is to compute straight running means of L consecutive values. Usually, simple sums which differ from the means by a factor are used to obviate division

by L. This smoothing, symbolically indicated by S_L, is then

$$Y_i = \sum_{j=i-L+1}^{i} X_i, \tag{27}$$

and has the power transfer function

$$S_L(f) = \left[\frac{\sin \frac{L\pi f}{2f_F}}{\sin \frac{\pi f}{2f_F}}\right]^2, \tag{28}$$

where f is the frequency and f_F is the folding frequency. $S_L(f)$ has periodic transmission nulls at $(f/f_F) = 2n/L$, where $n = 1, 2, \cdots$. Because the loss between nulls is usually not too great, a common procedure is to smooth twice with S_L followed by $S_{L\pm1}$ (indicated by $S_{L\pm1}S_L$); the second smoothing will have nulls tending to fall between those of the first.

The processing chosen for the present data was $F_2S_3F_4$ — smoothing by threes and fours and then retaining every other point. The new folding frequency is $250/2 = 125$ cps. The smoothing loss is plotted in Fig. 9 as a function of the fraction of the new folding frequency; the folded portion of the loss curve is also shown. Maximum loss occurs at 125 (near 120), 167 (near 180), and 250 cps. The loss peak at 125 will make it impossible to obtain accurate spectral estimates close to the folding frequency, but this is not serious. Spectra can now be computed with the same resolution, stability and duration of data, for one-fourth of the computer time.

XI. POWER SPECTRA

The method employed in determining power spectral estimates is that described by Blackman and Tukey;[2] another good reference is Ref. 5.

11.1 *Spectral Computation Parameters*

The spectra to be shown were computed using 5000 points (20 seconds at 250 samples/second). The mean and a least squares linear trend was removed from the data sections used, and the first and last 5 per cent of each section were raised cosine tapered to zero. The autocovariances (mean lagged products) were determined for 100 lags (i.e. for lags of $n\Delta t$, where $n = 0, 1, \cdots, 100$, and Δt is the sample spacing). A finite cosine transform of the autocovariances then provides spectral estimates $125/100 = 1.25$ cps apart from zero to the folding frequency. The spectra

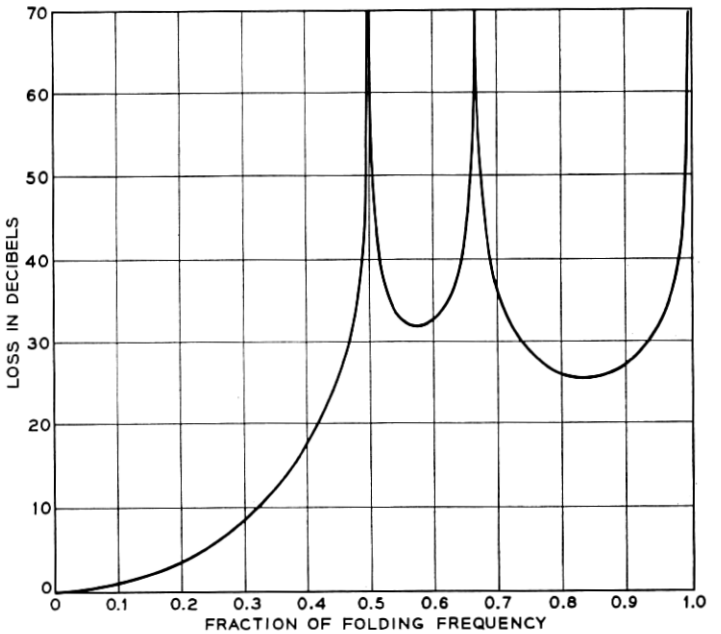

Fig. 9 — Smoothing loss for S_3S_4 vs fraction of folding frequency.

were smoothed by hanning (see Ref. 2, p. 98). Under these conditions, each estimate has a 90 per cent chance of being within about a 2-db range of the true spectrum. Or, the difference between the estimate and the true spectra has a variance of about $(0.3 \text{ db})^2$.

11.2 *Computed Spectra*

Almost fifty different spectra were computed from the data collected. A representative set of these are plotted (circles) on Figs. 10–16, where they may be compared to corresponding theoretical spectra. The comparison will be discussed later. All of the plotted spectra were equalized for the smoothing loss before plotting. It may be noted that most of the curves are not plotted beyond some frequency between 80–100 cps. The smoothing and decimating ($F_2S_3S_4$) produced an infinite-loss notch in the spectrum at 125 cps. When the spectrum is subsequently computed this hole is filled in by computation noise. The plot was automatically ended at the frequency where equalization of this noise started to produce a meaningless result. Even so, the last few points plotted are inaccurate and tend to be lower than they should be.

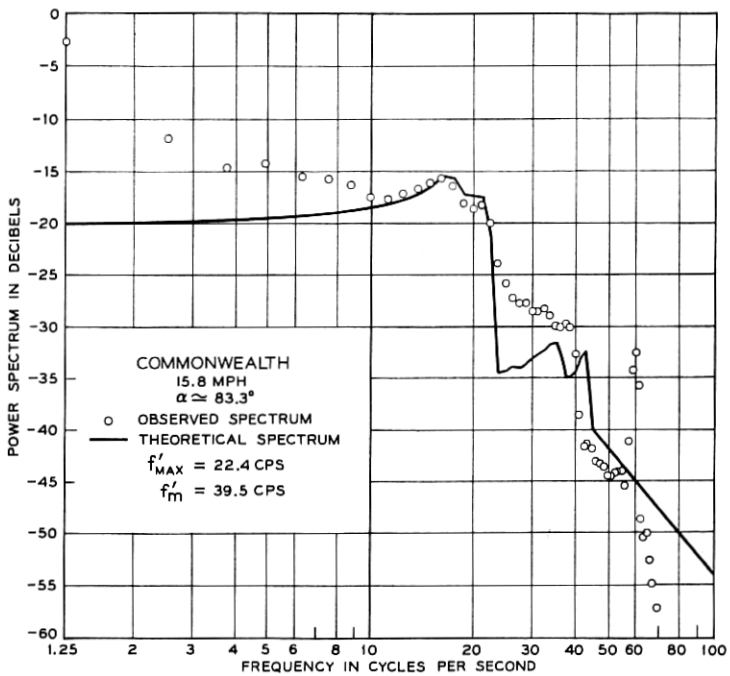

Fig. 10 — Experimental fading waveform spectrum compared with corresponding theoretical spectrum. Relative amplitudes are arbitrary; see discussion in text.

11.3 *Spectral Density Curve Shapes*

The spectra all exhibit significant power density out to some frequency between about 20 to 40 cps, where the density falls sharply between 10 and 15 db and then more gradually at about 12 db/oct. Many show a distinct shelf between the sharp-fall frequency and the subsequent slow fall-off. The shelf generally ends with a noticeable sharp drop at a frequency about twice the earlier sharp-fall frequency. The shelf in Fig. 14 has a noticeable peak prior to its fall at about 75 cps. The peak at 60 cps in all the plots is power supply hum. Another significant common feature is the relatively narrow peak immediately preceding the sharp-fall frequency. Many of the spectra exhibit a noticeable broad peak below the narrow one. All of the spectra rise 10 to 15 db at low frequencies.

XII. COMPARISON OF THEORETICAL AND EXPERIMENTAL SPECTRA

To compute a theoretical spectrum corresponding to a particular experimental spectrum, it is necessary to know the carrier frequency

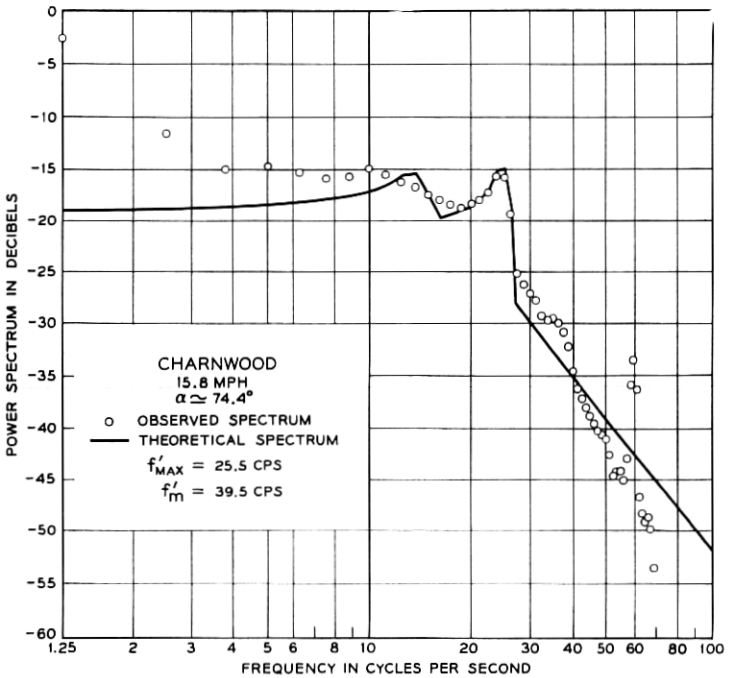

Fig. 11 — Experimental fading waveform spectrum compared with corresponding theoretical spectrum. Relative amplitudes are arbitrary; see discussion in text.

and vehicle speed in order to compute f_m, and to know the variation in the parameter angle α. For the present comparisons, the carrier frequency is 838.032 mc, and the average vehicle speed and corresponding f_m' are shown in Table I. The range of α's represented in the comparisons is from about 12° to 83°; remember that the spectrum for $\alpha = 90° + x$ is the same as one for $\alpha = 90° - x$. The weighting function W was limited to $W_{\max} = 15$ (compatible with the typical run length of 450 feet and typical house side length of 30 feet).

For each theoretical spectrum, the corresponding list of α's was used. Spectra were computed for each α and the final spectrum was the hanned weighted average. Harmonic power was included in each α's spectra before averaging. A value of $W_{\max} = 15$ was used in all cases. Table I also lists the $f_{\max}'$ corresponding to the value of α occurring during run that is nearest to 0° or 180°. As an example of how the list of α's was used, consider Commonwealth Avenue (case 1). These data are actually points 1–5000 (250 pts/sec) of a longer piece. The vehicle speed according to Table I was 15.8 mph; thus the run was (20 sec)(15.8 mph)(22

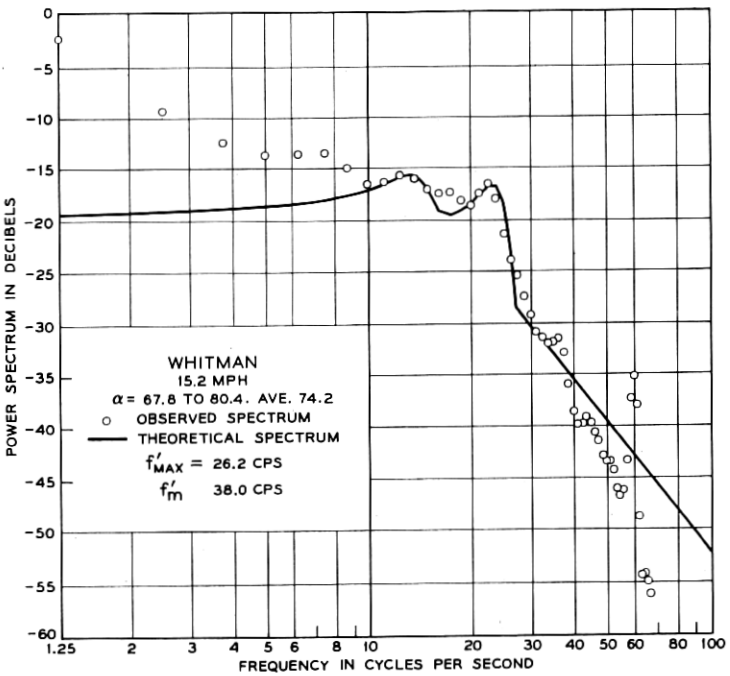

Fig. 12 — Experimental fading waveform spectrum compared with corresponding theoretical spectrum. Relative amplitudes are arbitrary; see discussion in text.

ft./sec)/(15 mph) = 463 ft. in length. The angles α_n are values computed for distances $d_n = 50\ n$ ft., where $n = 0, 1, 2, \cdots$ and may be considered to represent the distance ranges $d_n \pm 25$ ft. Thus the relative weights for the α_n and the corresponding spectra are $w_1 = 0.5$, w_2 to $w_9 = 1.0$, and $w_{10} = 0.76$; the latter is $(463 - 25 - 8.50)/50$. When the data section does not begin at sample 1, the distance between sample 1 and the starting sample must be determined using the proper average vehicle speed for that interval.

The change in α during the data section is small enough in many cases to permit using the average α to compute the spectrum. For example, during the run of case 4 the angle α varies only from 41.0° to 42.6°; a spectrum computed from the average value of about 41.8° differs little from one determined by averaging. In other cases — Whitman Road for example — the spectrum determined by averaging has much broader peaks than one corresponding to the average α. All the theoretical spectra to be shown were determined by averaging, whether this was necessary or not.

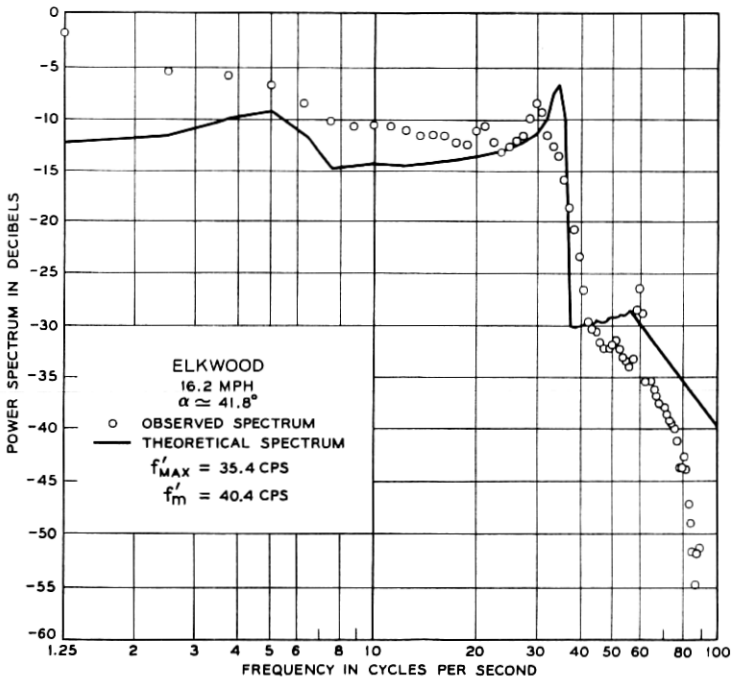

Fig. 13 — Experimental fading waveform spectrum compared with corresponding theoretical spectrum. Relative amplitudes are arbitrary; see discussion in text.

12.1 *Comparing Theoretical and Experimental Curves*

Figs. 10–16 show theoretical spectra (solid curves) superimposed on experimental spectra (circles); Table I lists the data sections involved and gives corresponding figure numbers. The only thing arbitrary in comparing the theoretical and experimental spectra is their relative amplitude. Thus the theoretical curve has been shifted vertically to produce some sort of fit. In all cases a transition is shown from the basic theoretical spectrum to a fall-off line fitted by least squares to the portion of the theoretical spectrum above f_{max}'; this fall-off typically has a slope of -12 to -13 db/oct. The last few points of each experimental curve are not very accurate and tend to be low, as previously discussed.

12.2 *General Results of the Comparison*

Before reading further, the reader should make a superficial scan of Figs. 10–16. The agreement between the theoretical and experimental spectra is generally quite good. The main discrepancy is that the ob-

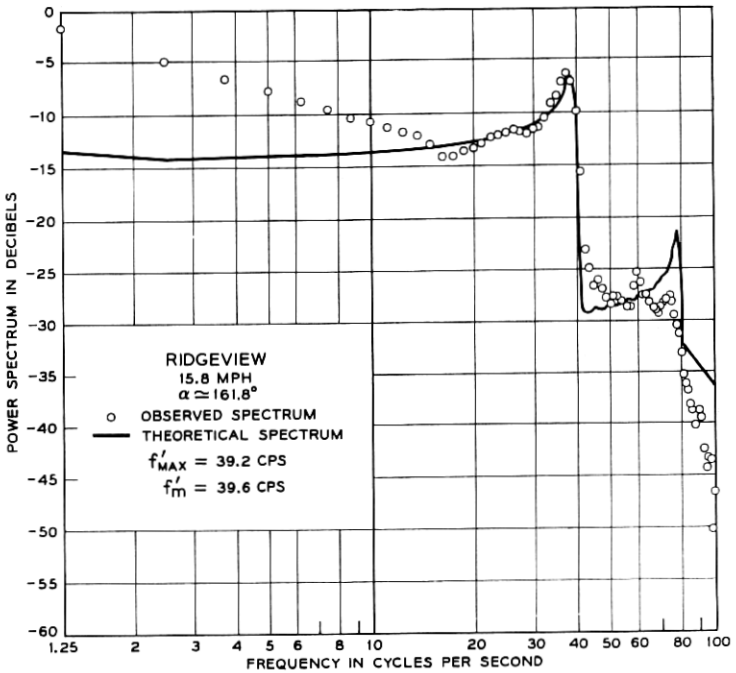

Fig. 14 — Experimental fading waveform spectrum compared with corresponding theoretical spectrum. Relative amplitudes are arbitrary; see discussion in text.

served rise in spectral density at low frequencies is not predicted by the theory. The sharp-fall frequency agrees very well in almost all cases. The peak prior to this sharp fall fits well in many cases. In cases where intermediate peaks are predicted (α not too close to zero), the experimental spectra usually exhibit them. The second harmonic shelf is well formed in many cases. The following are some comments on specific comparisons:

12.2.1 *Case 1; Fig. 10*

This street had an average α of about 83°. The two peaks have nearly merged and have formed a double peak which the experimental spectrum exhibits in agreement. The second-harmonic shelf is higher than predicted and ends somewhat early; more will be said about this later.

12.2.2 *Case 2; Fig. 11*

Here α averages about 74°. The upper peak and the sharp fall agree well. The intermediate peaks are in only fair agreement. Because of

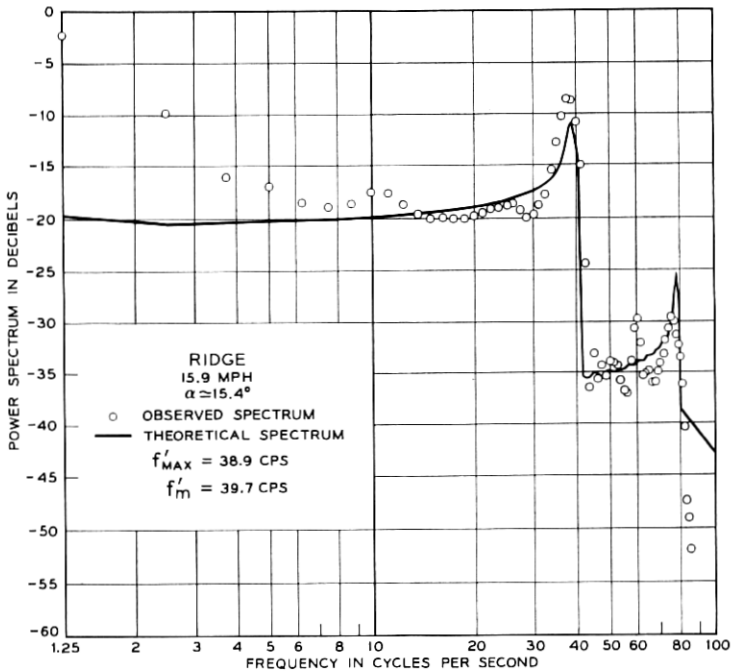

Fig. 15 — Experimental fading waveform spectrum compared with corresponding theoretical spectrum. Relative amplitudes are arbitrary; see discussion in text.

the absence of a second-harmonic shelf in the experimental spectrum, the theoretical fall-off line is plotted beginning with its intersection with the first fall. A slight rise above this line occurs out to nearly 40 cps; a second-harmonic shelf would have to extend to about 50 cps.

12.2.3 *Case 3; Fig. 12*

The comparison here is similar to that discussed for case 2. This street, however, has an α which varies between 67.8° and 80.4° and averages 74.7°. The comparatively broader theoretical and experimental peaks may be noted.

12.2.4 *Case 4; Fig. 13*

This street has α averaging about 42°. The intermediate peak at about 5 cps is discernible. The sharp fall occurs at about the right frequency but is not as steep as expected. The second-harmonic shelf is not noticeable. The theoretical fall-off line is picked up at its intersection with the theoretical shelf.

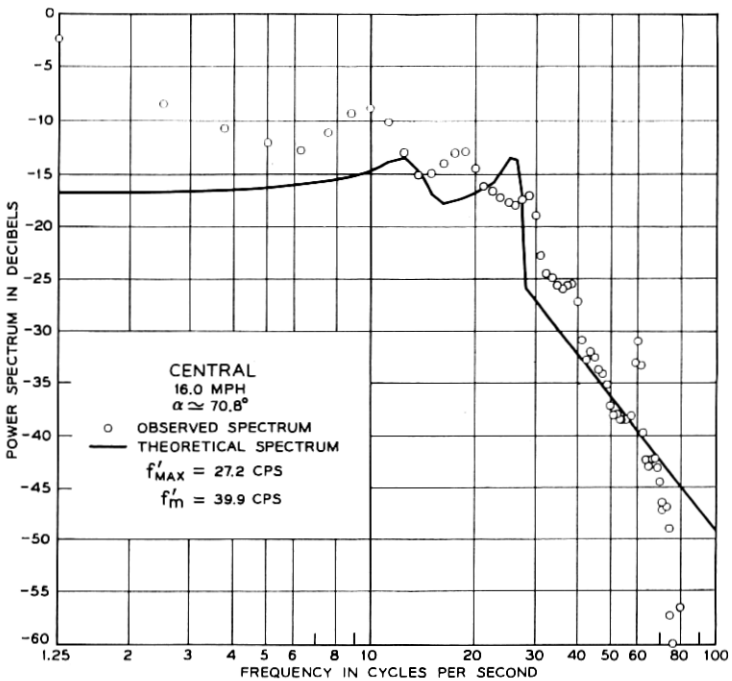

Fig. 16 — Experimental fading waveform spectrum compared with corresponding theoretical spectrum. Relative amplitudes are arbitrary; see discussion in text.

12.2.5 *Cases 5 and 6; Figs. 14 and 15*

These streets have a small α (about 12° and 15° respectively) and the intermediate peak is too close to zero frequency (below 1 cps) to show up with the present resolution. The main peak and the sharp fall agree exceptionally well and the second harmonic shelves are well exhibited. Furthermore, the predicted peak on the shelf appears in the experimental spectrum of Fig. 15 (and to a lesser extent in Fig. 14).

12.2.6 *Case 7; Fig. 16*

The agreement between the theoretical and experimental curves is in this case relatively poor. This street, however, is not in a suburban residential area, and has only a few low industrial buildings spaced well back from the curb. The section of the street corresponding to Fig. 16 had an average of α of about 71°. It was observed that, if experimental spectra were computed for other portions of the street with different α's, these spectra were quite similar if their ripples were ignored.

12.3 *Additional Observations*

It has been observed that the streets having the best agreement between experimental and theoretical spectra in the vicinity of the higher peak, sharp fall, and harmonic shelf are those with α near 0° or 180°. A good reason why this is not too surprising is offered in Section XIII under a discussion of nonrandom reflector orientation.

A cause for the small but discernible drop in Figs. 10, 11, 12 and 16 at the frequency corresponding to f_m' is offered in Section XIII under a discussion of simultaneous reflections.

When the harmonic content was included in the theoretical spectra it was assumed that the reflectors were perfect conductors. The observation of second-harmonic shelves at the predicted amplitude level in many cases indicates that the assumption was reasonable. The use of an aluminum foil vapor barrier integral with outside wall insulation is common in current house construction and may explain their good reflectivity.

XIII. LIMITATIONS OF THE MODEL

In the preceding section it was seen that a major deficiency of the theoretical model is its failure to forecast the rise in spectral density at the low-frequency end of the spectrum. Some of the mechanisms that can contribute low-frequency energy are discussed in the following paragraphs.

13.1 *Shadowing by Buildings*

The shadowing of the direct signal by buildings introduces into the fading waveform a low-frequency multiplicative function (likely with some harmonic content) with a fundamental spectrum probably not extending much beyond about ¼ cps (houses spaced 80–100 ft. apart and a vehicle speed of about 15 mph). The resulting fading waveform spectrum would be the convolution of the spectrum without shadowing with that of the low-frequency function. Such a low-frequency multiplicative function was observable in some portions of microfilm plots of recording fading waveforms. It is not likely that this effect explains the entire extent and shape of the low-frequency rise.

13.2 *Ground Reflections*

These cause standing-wave patterns which normally vary only in a vertical direction. But as the vehicle moves the point on the ground causing the ground reflection moves and the reflectivity will vary. This

and the shadowing of ground reflections by buildings introduce low-frequency variations in the direct signal.

13.3 *Simultaneous Reflections*

An assumption inherent in the construction of the theoretical spectra was that the mobile vehicle was under the influence of one reflector at a time. The simultaneous presence of more than one reflected signal will give rise to additional beat frequencies in the fading waveform between the reflected signals (see Section IV). Here the Doppler point of view is useful. From (14) the Doppler-shifted reflected signal is seen to lie in the frequency range $f_r = f_c \pm V/\lambda_c$; thus, if all possible reflections are always present, the radio frequency spectrum would have a bandwidth $2V/\lambda_c = f_m'$. The Doppler shifted direct signal has from (13) a frequency of $f_i = f_c + (V/\lambda_c) \cos \alpha$. The shape of the spectrum is not symmetrical about f_c. This shape can be obtained by picking frequencies f_r between $f_c - V/\lambda_c$ and $f_c + V/\lambda_c$, solving (14) for the two values of φ corresponding to each frequency, and then summing the two corresponding values of the weighting function W obtained from (18). The result is a spectrum having a broad minimum at $f_r = f_i = f_c + (V/\lambda_c) \cos \alpha$ and peaks at $f_r = f_i \pm V/\lambda_c$. Thus, as α varies from $\alpha = 0$ to 90° to 180°, the direct signal f_i moves from the upper-frequency end of the spectrum to the center and to the lower end. Fig. 17 shows the radio-frequency spectrum as a function of α (the peaks appear sharp because no smoothing has been applied). If the direct signal is large in amplitude compared to all the reflected signals, the spectrum of the envelope would essentially be that obtained previously (Section V), except for the lack of harmonic content. If the direct signal is ignored, the spectrum of the envelope would be the convolution of the radio-frequency spectrum with itself (see Ref. 6, Chap. 12); this spectrum, which would vary from a maximum at zero frequency to zero at $2V/\lambda_c$, would be virtually independent of α. The fact that the convolution would carry the spectra only out to $2V/\lambda_c$ suggests that beats between reflections may be responsible for the partial filling in of the second-harmonic shelf when α is not near 0 or 180°. This effect is noticeable to various degrees in Figs. 10, 11, 12 and 16, where a perceptible drop occurs at f_m' independent of any termination of the second-harmonic shelf at $2f_{max}'$. Similarly, this effect probably decreased the steepness of the observed steep fall in Fig. 13. It remains a fact that in a suburban residential environment, the spacing of houses is such that there is a very strong tendency for a mobile vehicle to experience only one domi-

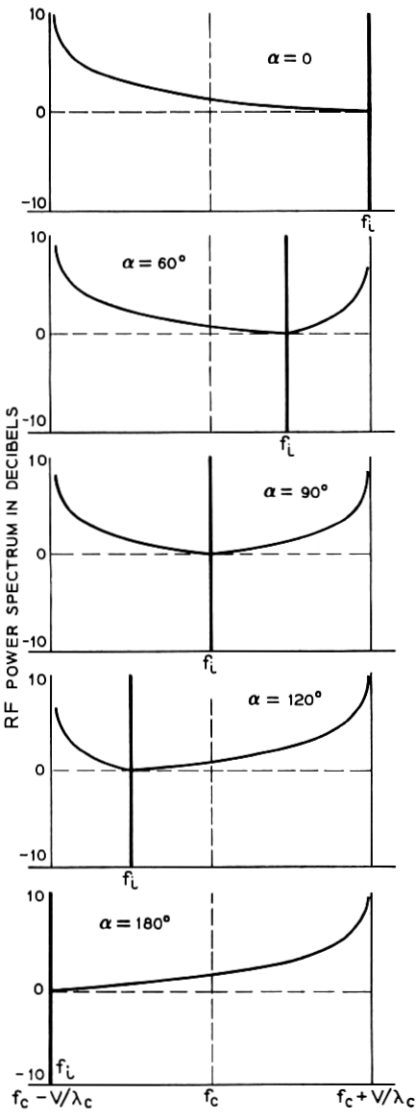

f_c = TRANSMITTED CARRIER FREQUENCY
λ_c = WAVELENGTH CORRESPONDING TO f_c
V = MOBILE STATION SPEED
f_i = DOPPLER SHIFTED DIRECT SIGNAL = $f_c + \frac{V}{\lambda_c} \cos \alpha$

Fig. 17 — Radio-frequency power spectra for a range of relative vehicle direction α.

nant reflection at a time. There certainly is some continual overlap of reflected beams and this may in part be responsible for the low-frequency rise in the experimental spectra.

13.4 *Nonrandom Reflector Orientation*

Houses are generally built with their larger flat sides parallel and perpendicular to the street. It has been shown from (11) that a zero fade rate obtains when $\varphi = 0°$, 2α, and 180°; low-frequency fades obtain when φ is near these values. The weighting function W is zero for $\varphi = 0°$ and 180° (except when $\alpha = 0°$ or 180°), but is unity at $\varphi = 2\alpha$. Clearly, it is the reflectors whose flat sides are roughly parallel to the direction of vehicle travel that contribute the low-frequency fade rates; each such reflector makes its contribution when the vehicle position is such that its $\varphi \approx 2\alpha$. Conventional house orientation obviously increases the supply of reflectors causing low-frequency fades above that under random conditions. It is felt that this effect may be the most important reason for the low-frequency rise in experimental fading spectra.

The same nonrandomness will affect the experimentally observed spectral peaks. These peaks occur when $\varphi = \alpha$ and $\alpha + 180°$; the corresponding required reflector orientations, relative to the direction α, are $\alpha/2$ and $90 - \alpha/2$. When α is small or near 180°, these required relative orientations are near 0° and 90° — i.e., near parallel and perpendicular to the direction of travel. When α is near 90°, the required relative orientations are both near 45°. Thus observed peaks for α's near 90° may be relatively subdued by the relative absence of required reflectors. This effect has been observed in several comparisons of theoretical and experimental spectra.

13.5 *Other Low-Frequency Effects*

Nonuniformity of the fixed station antenna pattern and reflectors in the vicinity of the fixed antenna can produce some very low-frequency variations in the standing wave pattern. Motion of the fixed antenna and trees due to wind are additional sources of low frequencies in the standing wave pattern.

XIV. ADDITIONAL TOPICS

14.1 *Moving Reflectors*

All of the preceding discussion was concerned with fixed reflecting objects. The experimental data were taken with the streets devoid of

other moving vehicles. What effect will the motion of other vehicles have on the spectrum? Let us limit this discussion to vehicles moving in the same or opposite direction on the same street as the mobile station; let V_1 and V_2 be the speeds of the mobile station and moving reflector respectively with a positive V_2 corresponding to closure between the vehicles. The moving reflector encounters and reflects a frequency

$$f_2 = f_c - \frac{V_2 \cos \alpha}{\lambda_c}, \tag{29}$$

where f_c, λ_c, and α have their previous meanings, and V_2 has a component away from the fixed station. The mobile station encounters a reflected beam of frequency

$$f_1 = f_2 + \frac{V_1 + V_2}{\lambda_2}, \tag{30}$$

where λ_2 corresponds to f_2, and encounters a Doppler shifted direct signal of frequency f_i given by (13). The beat frequency f between f_i and f_1 is then

$$\begin{aligned} f = f_1 - f_i &= f_2 + \frac{V_1 + V_2}{\lambda_2} - f_c - \frac{V_1 \cos \alpha}{\lambda_c} \\ &= \frac{V_1 + V_2}{\lambda_2} - \frac{(V_1 + V_2) \cos \alpha}{\lambda_c} \\ &\approx \frac{V_1 + V_2}{\lambda_c} (1 - \cos \alpha), \end{aligned} \tag{31}$$

where c is the velocity of light. This result corresponds to (16) with $\varphi = \alpha$. Thus an oncoming vehicle with $V_2 = V_1$ could double the maximum observed fade rate.

14.2 *Horizontal Polarization*

In terms of the x and z coordinates of Fig. 1, the electric field components in the reflected beam region will take the form (see Ref. 1, p. 295)

$$E_x = jK \cos \theta \sin \left(\frac{2\pi z}{\lambda_c} \cos \theta \right) \exp \left(-j \frac{2\pi x \sin \theta}{\lambda_c} \right) \tag{32}$$

$$E_z = K \sin \theta \cos \left(\frac{2\pi z}{\lambda_c} \cos \theta \right) \exp \left(-j \frac{2\pi x \sin \theta}{\lambda_c} \right), \tag{33}$$

where K is a constant and θ is the angle of incidence. If a nondirectional

receiving antenna is used, such as is approximated by a "turnstile" consisting of two perpendicular dipoles connected together by a $\lambda_c/4$ stub, the received signal can be shown to be proportional to

$$| E | = \left| K \sin \left(\frac{2\pi z}{\lambda_c} \cos \theta - \theta \right) \right| \tag{34}$$

irrespective of the angular orientation of the turnstile. This result has the same form as (25) except for the spatial phase shift θ. Thus the use of horizontal polarization together with the assumed antenna produces an effective standing-wave pattern that is identical to that for vertical polarization except for the spatial translation. Thus the fading situation would also be identical.

14.3 *Field Component Diversity*

Equations (32) and (33) show that E_z is a maximum where E_x is zero and conversely. Suppose the two dipoles of the turnstile antenna are not connected together with a stub but are offered simultaneously to the receiver. Then, if the receiver electronically switched to the dipole offering the greater signal, the receiver would in many cases never experience a null. However, when the direction to the reflector φ approaches 180°, θ approaches 0° and the component E_z becomes smaller and vanishes; likewise, E_x vanishes when φ approaches 0. Thus any diversity scheme dependent on choosing between E_x and E_z would be most successful near $\varphi = 90°$ ($\theta = 45°$) and unsuccessful near $\varphi = 0°$ or 180° ($\theta = 90°$ or 0°).

At every point in the reflected beam region it would be possible to rotate a dipole to a position where a maximum signal is picked up. This is not possible only when $\varphi = 0°$ or 180° exactly. It is possible, therefore, for a mobile dipole that is mechanically or electronically rotated continuously to receive a maximum signal, to reduce the amplitude of the fading due to vehicle motion, if horizontal polarization is employed. If the angular position of a mobile single dipole is fixed, the fundamental fading rate experienced is still the same function of α and φ as before, except that the amplitude of the fading will vary because of the directivity of the dipole. For example, if $\varphi = 90°$ and the dipole is physically oriented perpendicular to the fixed station, the mobile dipole may be translated anywhere in the reflected beam region without any fading.

XV. ACKNOWLEDGMENTS

Much credit is due J. L. Wenger and H. H. Hoffman for their part in recording the raw data; the former skillfully manned the fixed station

equipment at Murray Hill and the latter operated the mobile equipment and had the difficult job of driving the Volkswagen at something approaching a constant speed. Thanks are due C. A. Sjursen and J. L. Wenger for their part in digitizing the data. Miss A. B. Strimaitis made the Visicorder record measurements. The direction of this effort benefited from B. P. Bogert's experience in time series analysis.

REFERENCES

1. Ramo, S., and Whinnery, J. R., *Fields and Waves in Modern Radio*, John Wiley & Sons, New York, 1953.
2. Blackman, R. B., and Tukey, J. W., *The Measurement of Power Spectra*, Dover Publications, Inc., New York, 1959.
3. Healy, M. J. R., and Bogert, B. P., FORTRAN Subroutines for Time Series Analysis, Comm. ACM, **6**, Jan., 1963.
4. David, E. E., Mathews, M. V., and McDonald, H. S., Hi-Speed Data Translator for Computer Simulation of Speech and Television Devices, Proc. Western Joint Computer Conf., Mar., 1959.
5. Technometrics, **3**, May, 1961.
6. Davenport, W. B., and Root, W. L., *Random Signals and Noise*, McGraw-Hill Book Co., New York, 1958.